Electron transport through Al–ZnO–Al: An *ab initio* calculation

Zijiang Yang,[1] Langhui Wan,[1] Yunjin Yu,[1] Yadong Wei,[1,2,a)] and Jian Wang[2]
[1]*School of Physics Science and Technology and Institute of Computational Condensed Matter Physics, Shenzhen University, Shenzhen 518060, People's Republic Of China*
[2]*Department of Physics, The University of Hong Kong, Pokfulam Road, Hong Kong, People's Republic of China*

(Received 7 April 2010; accepted 24 June 2010; published online 4 August 2010)

The electron transport properties of ZnO nanowires coupled by two aluminum electrodes were studied by *ab initio* method based on nonequilibrium Green's function approach and density functional theory. A clearly rectifying current-voltage characteristics was observed. It was found that the contact interfaces between Al–O and Al–Zn play important roles in the charge transport at low bias voltage and give very asymmetric I-V characteristics. When the bias voltage increases, the negative differential resistance occurs at negative bias voltage. The charge accumulation was calculated and its behavior was found to be well correlated with the I-V characteristics. We have also calculated the electrochemical capacitance which exhibits three plateaus at different bias voltages which may have potential device application. © *2010 American Institute of Physics*. [doi:10.1063/1.3467000]

I. INTRODUCTION

The investigations on ZnO material have been continued for many decades due to its wide range of applications.[1] Due to its large direct band gap ($E_g \sim 3.3$ eV at 300 K) and large exciton binding energy ~60 meV (room-temperature 300 K is about ~25 meV), it is an important material for manufacturing ultraviolet devices[2] and high temperature luminescent devices.[3,4] Its easy growth with high purity makes it a low cost material as high quality substrate[5,6] and its easily etched property makes it possible to be made as small-size devices. It can be used as space devices[7] and transparent thin-film transistors[8,9] because of its insensitivity to high energy radiation and visible light. It can also be a candidate as a spintronic material because Mn-doped ZnO, as well as Fe-, Co-, or Ni-alloyed ZnO, has high Curie temperature ferromagnetism.[10] There are many other properties and applications for ZnO bulk material and ZnO related materials that make ZnO a unique material for emerging nanotechnology.[1]

Recently, several configurations of ZnO nanostructures such as nanowires,[11] nanotubes,[12–14] nanobelts,[15,16] nanosheets,[17,18] and nanorods,[12,14] have attracted much attention due to their potential applications and easy fabrication.[19] Such ZnO nanostructures have novel electrical[20–22] and optoelectrical[23,24] properties as well as mechanical properties.[19] They can be used to make sensitive chemical nanosensors,[25,26] solar cell,[27] light-emitting devices,[28,29] nanogenerators (converting nanoscale mechanical energy into electricity), and nanopiezotronic devices.[19] First principles calculations for the geometry and electronic structure of small ZnO nanowire and nanobelt were also carried out by many authors.[16,30,31] More recently, the carrier transport of ZnO coupled by metal layers such as Au electrode and Mg electrode were studied by Kamiya.[32] In their calculation, it was found that the Au–ZnO–Au interface shows Schottky contact behavior while the Mg–ZnO–Mg interface shows Ohmic contact. The contact behavior has crucial influence on the device property and is very sensitive to the fabrication processes.[33] Hence it is very useful to study the contact behaviors between ZnO and other materials. In addition, it is very useful to study other transport properties such as charge polarization and electrochemical capacitance. In this paper, we concentrated on the transport behaviors and charge distribution and charge accumulation of Al–ZnO–Al molecular structure by the density functional theory (DFT) combined with nonequilibrium Green's function method. Different from Au–ZnO–Au and Mg–ZnO–Mg nanostructures, we found that for Al–ZnO–Al molecular junction the I-V curve is highly asymmetric. In addition, a negative differential resistance appears at negative bias voltage. Furthermore, we have calculated the electrochemical capacitance C_μ of this device and found that C_μ depends on bias voltage in a unique way: there exists three regions where C_μ is constant. At small bias, our analysis shows that electrochemical capacitance is dominated by the classical capacitance whereas at large bias voltage quantum effect becomes important.

II. METHOD

Here we present our first principles analysis of electronic transport through a Al–ZnO–Al nanodevice. The calculation package we used is NADCAL (Ref. 34) [the developed code of MCDCAL (Ref. 35)], which is an implementation of real space DFT within the Keldysh nonequilibrium Green's function formalism (NEGF). The DFT method provides the system electronic structure and NEGF includes information of the nonequilibrium quantum statistics. The system we studied was a typical two-probe open system which was divided into a scattering region and two semi-infinite electrodes. The electronic structure of the central region was calculated self-consistently and the couplings between the central region and the two semi-infinite electrodes were included by the

a)Electronic mail: ywei@szu.edu.cn.

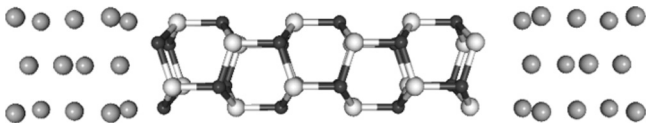

FIG. 1. Schematic plot of Al–ZnO–Al (Al: gray; Zn: white; O: black). The direction from left to right is considered as z-axis.

self-energy. Enough buffer layers for Al atomic electrode were included in the central region so that the boundary conditions of the scattering region could be determined through the corresponding infinite left and right electrodes. We refer to Refs. 35–37 for detailed description of NEGF-DFT technique.

Our central scattering region consisted of six-layers of (0001) ZnO with width 3.752 Å and three buffer layers of each aluminum electrodes (see Fig. 1). Each ZnO layer had three oxygen atoms and three zinc atoms. Basis set was composed of s, p, d real space linear combination atomic orbitals. $3d^{10}4s^2$ was chosen as valence electrons for zinc and $2s^22p^4$ for oxygen. Exchange correlation was treated using LDA_PZ.[38] When solving the Poisson equation in real space one grid point occupied a volume of 4.583×10^{-3} Å^3. In the self-consistent calculation, the tolerance was set to be less than 10^{-4} hartree.

For Al–ZnO–Al structure in Fig. 1, the left electrode was coupled directly to oxygen atoms (Al–O contact) and the right electrode was coupled to zinc atoms (Al–Zn contact). Instead of relaxing ZnO and aluminum electrodes, we determined the distances between ZnO and electrodes by finding the minimum of total energy when changing the distance of Al–O and Zn–Al, respectively. According to Fig. 2 we set the distance between aluminum electrode and oxygen side of ZnO to be 1.95 Å while the distance of Zn–Al to be 2.75 Å.

For the two-probe NEGF+DFT formalism, the electronic current can be obtained by Landauer–Büttiker formula

$$I=\frac{2q}{h}\int dE\ \mathrm{Tr}[\hat{T}(E,V_L,V_R)](f_L(E,\mu_L)-f_R(E,\mu_R)), \quad (1)$$

where $\hat{T}(E,V_L,V_R)$ is the transmission matrix and is obtained by Green's function from the following formula:

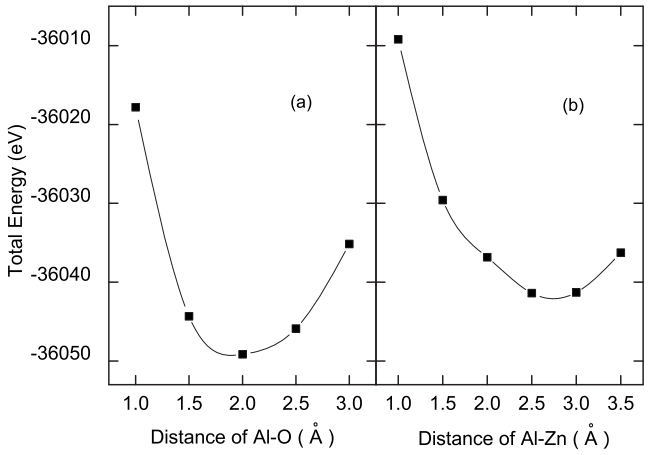

FIG. 2. Contact distances between aluminum electrode and ZnO determined by finding the lowest energy. (a) Total energy vs the distance between Al–O contact. (b) Total energy vs the distance between Zn–Al contact.

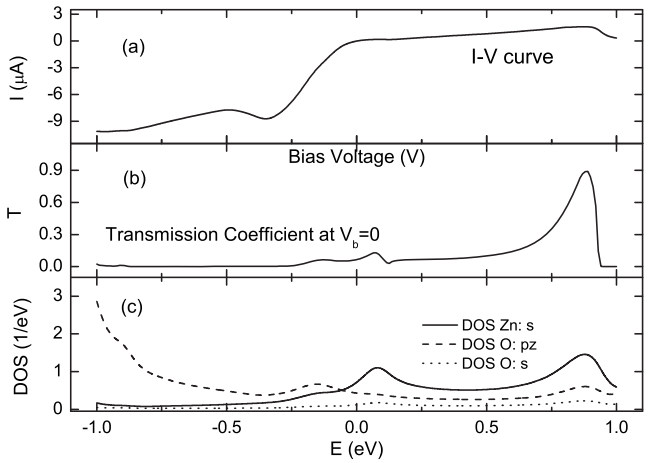

FIG. 3. (a) Current as a function of bias voltage $V_b=V_L-V_R$; (b) transmission coefficient vs energy at bias voltage $V_b=0$; (c) DOS vs energy due to zinc 4s state (Zn:s solid line), oxygen 2p state in z-direction (O:p_z dashed line), and oxygen 2s state (O:s dotted line).

$$\hat{T}(E,V_L,V_R)=\Gamma_L G^r \Gamma_R G^a. \quad (2)$$

$f_{L/R}=\{1+\exp[(E-\mu_{L/R})/kT]\}^{-1}$ is the Fermi distribution function of left/right electron reservoir connected to the left/right electrode at infinite $z=-\infty/\infty$. $\mu_{L/R}=\mu_{l/r}+qV_{L/R}$ is the electrochemical potential with $\mu_{l/r}$ the chemical potential of left/right lead and $V_{L/R}$ the applied potential on the left/right lead.

III. RESULTS AND DISCUSSIONS

In Fig. 3, we plotted the current-voltage (I-V) curve of Al–ZnO–Al. A rectifying I-V characteristics is clearly observed. The current increases slowly with increasing of the positive bias voltage V_b but decreases quickly when the bias voltage reverses its sign. Different behaviors of I-V characteristics when the bias voltage changes from positive to negative can be understood as follows. At zero temperature and in hartree unit, Eq. (1) becomes (we set $V_R=0$ in our calculation)

$$I=2\int_{-V_b}^{0}\frac{dE}{2\pi}\mathrm{Tr}\ \hat{T}(E,V_b). \quad (3)$$

We find that when the positive bias voltage is applied, the current is contributed from the energy integral interval $E=(-|V_b|,0)$. But for negative voltage $V_b<0$, the transmission coefficient will be integrated on the positive interval $E=(0,|V_b|)$. Although the transmission coefficient is a function of the bias voltage, we first analyze the I-V curve near $V_b=0$. For this purpose, we plotted the transmission coefficient and the density of states (DOS) versus the Fermi energy at $V_b=0$ in Fig. 3. In our calculation we find that three kinds of states give major contributions to the I-V curve. They are zinc 4s-orbital, oxygen z-component of 2p-orbital, and oxygen 2s-orbital. Among them, contribution due to oxygen 2s-orbital is the smallest so we focus on the other two orbits. It is clear that when $E>0$ the DOS of zinc s-orbital is much larger than that of oxygen p_z-orbital and when $E<0$ both zinc s-orbital and oxygen p_z-orbital contribute near $E=0$ but the contribution is less than that of the zinc s-state at $E>0$.

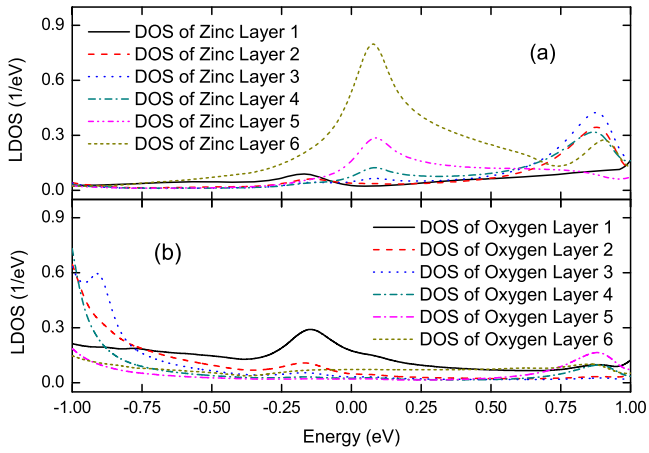

FIG. 4. (Color online) (a) Local DOS of zinc 4*s*-state on each layer; (b) local DOS of oxygen p_z-state on each layer.

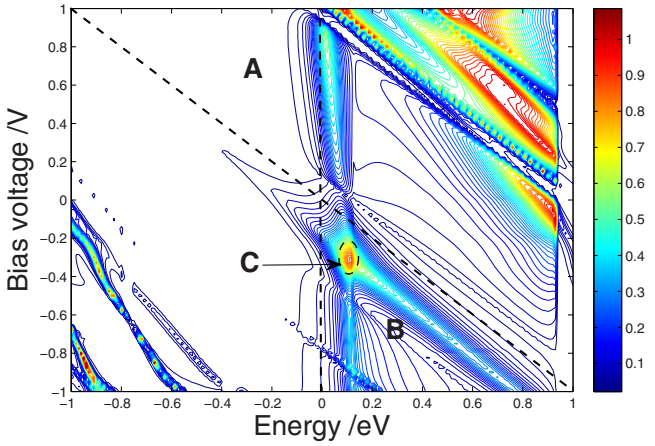

FIG. 5. (Color online) Transmission coefficient vs bias voltage V_b and energy E. The dashed black lines are only used as symbol lines in order to depict the region A, B, and C.

So we conclude that when negative bias voltage is added electrons pass device mainly from zinc *s*-orbital but when the positive bias voltage is added electrons pass device mainly from both zinc *s*-orbital and oxygen p_z-orbital. To provide further evidence, we analyze the local DOS (LDOS) according to the layers of ZnO in the scattering region (see Fig. 4). Note that we label the layers of oxygen and zinc from left to right. One can find that each layer has very different LDOS. For zinc atoms, the rightmost layer (the layer 6, i.e., the layer coupled directly to aluminum lead) gives the largest LDOS around the Fermi level. (The Fermi level is shifted to $E=0$ in our calculation.) When the energy increases the LDOS of middle layers (layers 2 to 4) gradually increase and reach their maxima at about $E=0.83$ eV. But the LDOS of all zinc layers becomes small when $E<-0.25$ eV. For oxygen atoms, similar result is found if we recall that the first oxygen layer is connected directly to the left aluminum electrode. The LDOS of oxygen give the largest value at the first oxygen layer around the Fermi level $E=0$. When E becomes quite small and close to $E=-1.0$ eV, the LDOS of the middle layers (layer 3 and layer 4) dominate and when $E>0$ the LDOS of oxygen are small compared with the those of $E<0$. In other words, when small negative bias voltage is applied the contact interface between Al–Zn dominates I-V behavior. But when the positive bias voltage is applied, both Al–Zn interface and Al–O interface will dominate the charge transport. The rectifying behavior is mainly controlled by the contact interface characteristics due to the different coupling atoms Al–Zn and Al–O when bias voltage is small.

Actually the transmission coefficient $T=\mathrm{Tr}[\hat{T}(E,V_b)]$ is a function of the bias voltage $V_b=V_L-V_R$ at zero temperature so the situation becomes more complicated at large V_b. In Fig. 5, the transmission coefficient as a function of the energy E and the bias voltage V_b was depicted. The I-V curve for positive bias voltage corresponds to the triangular area A between the vertical line $E=0$ and the slope line $V_b=-E$ for bias voltage $V_b>0$ and energy $E<0$ (see the dashed black lines in Fig. 5) and the I-V curve for negative bias voltage corresponds to the triangular area B between the above two lines for $V_b<0$ and $E>0$. We find that in the right low triangular area B the transmission coefficient is much large within the interval $V_b\in(-0.4,-0.2)$ V and reach maximum around $V_b\sim-0.35$ V (see the C region in Fig. 5). That is why the absolute current value decreases when the absolute value of bias voltage increases around $V_b\in(-0.5,-0.35)$ V and the negative differential resistance appears in that voltage region [see I-V curve on the interval $(-0.5,-0.35)$ V in Fig. 3(a)].

For the quantum devices, due to finite DOS the charge accumulation in the scattering region differs from the charge accumulation in the classical metal capacitance and one should use the concept of electrochemical capacitance $C_\mu=\Delta Q/\Delta\mu$, where $\Delta\mu$ is the electrochemical potential difference between the two electron reservoirs[39–41] and the ΔQ is the charge accumulation. For our two-probe problem, both electrodes are aluminum so that $\mu_l=\mu_r$. Hence, at zero temperature, we have $\Delta\mu=V_b=V_L-V_R$. When the bias voltage is applied, the electrochemical potential across two probes is changed by $\Delta\mu=V_b$ from equilibrium, charges will be injected into the scattering region. The induced charges will occur due to the electron-electron interaction. In DFT, the injected and induced charges are automatically considered by solving the Kohn–Sham equation and the Poisson equation self-consistently and the Gauge invariant is also satisfied automatically.[42] Such a charge accumulation is closely related to the I-V characteristics and can only be determined by solving scattering problem. For a rough estimate, we divide the system into two parts from the middle of scattering region called left region and right region. We then calculate the charge accumulation $\Delta Q_L(V_b)=Q_L(V_b)-Q_L(0)$ and $\Delta Q_R(V_b)=Q_R(V_b)-Q_R(0)$ and plot them in Fig. 6. The electrochemical differential capacitance $C_\mu=dQ/dV_b$ was also plotted in Fig. 6. Here, Q is the fitted curve of $\Delta Q_R(V_b)$. Following observations are in order. First of all, the electrochemical capacitance depends on the voltage although it is a piecewise constant in three regions labeled as (a), (b), and (c). Second, the asymmetry of electrochemical capacitance C_μ is clearly seen. In region (a) which is asymmetric with respect to the bias voltage $V_b=(-0.27,0.01)$ V the electrochemical capacitance assumes a smaller constant value $C_\mu=0.003$ aF. While in region (b) and (c), C_μ are approximately four times larger. The value of the electrochemical

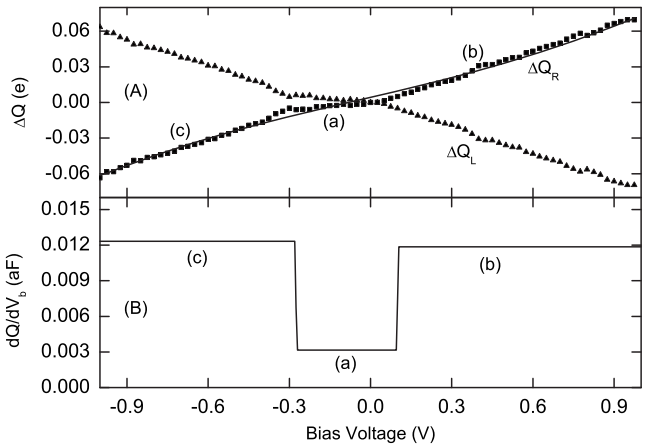

FIG. 6. (a) Charge accumulations vs bias voltage on left scattering region (ΔQ_L: triangles) and right scattering region (ΔQ_R: squares). The black solid line $Q(V_b)$ is the fitted curve of ΔQ_R; (b) electrochemical differential capacitance dQ/dV_b vs bias voltage.

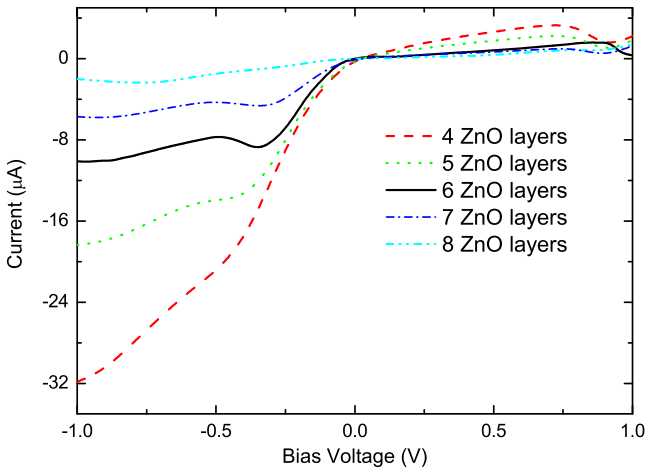

FIG. 7. (Color online) The I-V curve for Al–ZnO–Al structure with ZnO layers L_N=4,5,6,7,8.

capacitance also exhibits asymmetry between region (b) and (c). Finally, the behavior of electrochemical capacitance in region (a) can be understood *qualitatively* as follow. Since in region (a) the current is small, we can use the following formula for electrochemical capacitance (where the current is assumed to be zero)[43]

$$\frac{1}{C_\mu} = \frac{1}{C_0} + \frac{1}{e^2 D_L} + \frac{1}{e^2 D_R}, \tag{4}$$

where C_0 is the classical capacitance which can be roughly estimated using the parallel plate capacitor $C_0 = \epsilon_0 A/d \sim 0.002$ aF, where A is the cross-section area and d is the separation of two plates. Here D_L and D_R are the DOS of the left and right regions, respectively. From Fig. 4, we see that D_L and D_R are much larger than C_0/e^2 and hence can be neglected in Eq. (4). Therefore, we conclude that in region (a), the electrochemical capacitance is dominated by the classical capacitance. In region (b) and (c), however, quantum effect must be considered. At the moment, there is no analytic formula to account for the electrochemical capacitance at the nonlinear bias voltage.

In our calculations, we did not consider the influence of defects or impurities. The existence of such disorders is one of the main reasons for the difference between the theoretical results and the experimental data. But as long as the disorders do not change the distribution of the DOS significantly, the results of our calculations will remain unchanged. To investigate the effect of length of ZnO layers L_N on transport properties, we have calculated the I-V curve for L_N =4,5,6,7,8, where L_N=6 has been studied in detail in Figs. 1–6. In Fig. 7, we have plotted I-V curve for different L_N. It shows that for positive bias, the I-V curves are almost the same especially for large L_N while for negative bias all curves exhibit qualitatively the same feature.

In summary, we have analyzed the electron transport through the Al–ZnO–Al atomic junction and clear rectifying characteristic was observed. It was found that the contact interfaces between aluminum electrodes and central device ZnO play essential roles in the current-voltage behaviors when the bias voltage is small. When the negative bias voltage is applied, the major contribution to the electron transport comes from Zn *s*-states. But when the positive bias voltage is applied, both Zn *s*-state and O p_z-state are responsible in the charge transport. The negative differential resistance was found in our device. Our results showed that for such a quantum open system the charge accumulations in the scattering region are closely correlated with the applied bias voltage and I-V characteristics. The electrochemical capacitance was found to have three plateaus. At small bias, the electrochemical capacitance is dominated by the classical capacitance. At large bias, however, quantum effect becomes important. Our findings may have potential device application for future nanotechnology.

ACKNOWLEDGMENTS

We gratefully acknowledge support by a RGC grant from the Government of HKSAP under Grant No. HKU 704308P and the grant from the National Natural Science Fundation of China (Grant No. 10947018).

[1]Ü. Özgür, Y. I. Alivov, C. Liu, A. Teke, M. A. Reshchikov, S. Doğan, V. Avrutin, S.-J. Cho, and H. Morkoc, J. Appl. Phys. **98**, 041301 (2005).
[2]Z. K. Tang, G. K. L. Wong, P. Y. M. Kawasaki, A. Ohtomo, H. Koinuma, and Y. Segawa, Appl. Phys. Lett. **72**, 3270 (1998).
[3]C. X. Xu, X. W. Sun, X. H. Zhang, L. Ke, and S. J. Chua, Nanotechnology **15**, 856 (2004).
[4]A. M. Fischer, S. Srinivasan, R. Garcia, F. A. Ponce, S. E. Guaõ, B. C. Di Lello, F. J. Moura, and I. G. Solrzano, Appl. Phys. Lett. **91**, 121905 (2007).
[5]D. C. Look, Mater. Sci. Eng., B **80**, 383 (2001).
[6]E. Ohshima, H. Ogino, I. Niikura, K. Maeda, M. Sato, M. Ito, and T. Fukuda, J. Cryst. Growth **260**, 166 (2004).
[7]S. O. Kucheyev, J. S. Williams, C. Jagadish, J. Zou, C. Evans, A. J. Nelson, and A. V. Hamza, Phys. Rev. B **67**, 094115 (2003).
[8]H. S. Bae, M. H. Yoon, J. H. Kim, and S. Im, Appl. Phys. Lett. **83**, 5313 (2003).
[9]Y. Kwon, Y. Li, Y. W. Heo, M. Jones, P. H. Holloway, D. P. Norton, Z. V. Park, and S. Li, Appl. Phys. Lett. **84**, 2685 (2004).
[10]T. Dietl, H. Ohno, F. Matsukura, J. Cibert, and D. Ferrand, Science **287**, 1019 (2000).
[11]Y. W. Heo, D. P. Norton, L. C. Tien, Y. Kwon, B. S. Kang, F. Ren, S. J. Pearton, and J. R. LaRoche, Mater. Sci. Eng. R. **47**, 1 (2004).
[12]Q. C. Li, V. Kumar, Y. Li, H. T. Zhang, T. J. Marks, and R. P. H. Chang, Chem. Mater. **17**, 1001 (2005).
[13]L. Shi, Y. Xu, and Q. Li, Curr. Nanosci. **5**, 262 (2009).
[14]M. Riaz, A. Fulati, G. Amin, N. H. Alvi, O. Nur, and M. Willander, J.

Appl. Phys. **106**, 034309 (2009).
[15]Z. Pan, Z. Dai, and Z. Wang, Science **291**, 1947 (2001).
[16]J. Yang, S. Li, Y. Zhao, and X. Zhao, J. Phys. Chem. C **113**, 4804 (2009).
[17]A. Umar and Y. B. Hahn, Nanotechnology **17**, 2174 (2006).
[18]A. E. Suliman, Y. W. Tang, and L. Xu, Sol. Energy Mater. Sol. Cells **91**, 1658 (2007).
[19]Z. Wang, Mater. Sci. Eng. R. **64**, 33 (2009).
[20]Z. Fan, D. Wang, P.-C. Chang, W.-Y. Tseng, and J. G. Lu, Appl. Phys. Lett. **85**, 5923 (2004).
[21]C. S. Lao, J. Liu, P. Gao, L. Zhang, D. Davidovic, R. Tummala, and Z. L. Wang, Nano Lett. **6**, 263 (2006).
[22]X. Wang, J. Song, J. Liu, and Z. Wang, Science **316**, 102 (2007).
[23]H. T. Ng, B. Chen, J. Li, J. Han, M. Meyyappan, J. Wu, S. X. Li, and E. E. Haller, Appl. Phys. Lett. **82**, 2023 (2003).
[24]C. Soci, A. Zhang, B. Xiang, S. A. Dayeh, D. P. R. Aplin, J. Park, X. Y. Bao, Y. H. Lo, and D. Wang, Nano Lett. **7**, 1003 (2007).
[25]Q. Wan, Q. H. Li, Y. J. Chen, T. H. Wang, X. L. He, J. P. Li, and C. L. Lin, Appl. Phys. Lett. **84**, 3654 (2004).
[26]Z. Fan and J. G. Lu, Appl. Phys. Lett. **86**, 123510 (2005).
[27]M. Law, L. E. Greene, J. C. Johnson, R. Saykally, and P. Yang, Nature Mater. **4**, 455 (2005).
[28]C. Liu, J. A. Zapien, Y. Yao, X. Meng, C. S. Lee, S. Fan, Y. Lifshitz, and S. T. Lee, Adv. Mater. (Weinheim, Ger.) **15**, 838 (2003).
[29]M. H. Huang, S. Mao, H. Feick, H. Yan, Y. Wu, H. Kind, E. Weber, R. Russo, and P. Yang, Science **292**, 1897 (2001).
[30]J. E. Jaffe, J. A. Snyder, Z. Lin, and A. C. Hess, Phys. Rev. B **62**, 1660 (2000).
[31]P. Erhart, K. Albe, and A. Klein, Phys. Rev. B **73**, 205203 (2006).
[32]T. Kamiya, K. Tajima, K. Nomura, H. Yanagi, and H. Hosono, Phys. Status Solidi A **205**, 1929 (2008).
[33]K. Ip, G. T. Thaler, H. Yang, S. Y. Han, Y. Li, D. P. Norton, S. J. Pearton, S. Jang, and F. Ren, J. Cryst. Growth **287**, 149 (2006).
[34]NanoAcademic Technologies Inc. http://www.nanoacademic.ca/
[35]J. Taylor, H. Guo, and J. Wang, Phys. Rev. B **63**, 245407 (2001).
[36]J. Taylor, H. Guo, and J. Wang, Phys. Rev. B **63**, 121104(R) (2001).
[37]J. Wang and H. Guo, Phys. Rev. B **79**, 045119 (2009).
[38]J. P. Perdew and A. Zunger, Phys. Rev. B **23**, 5048 (1981).
[39]M. Büttiker, J. Phys.: Condens. Matter **5**, 9361 (1993)
[40]J. Wang, H. Guo, J. S. Mozos, C. C. Wan, G. Taraschi, and Q. R. Zheng, Phys. Rev. Lett. **80**, 4277 (1998).
[41]Y. D. Wei, X. A. Zhao, B. G. Wang, and J. Wang, J. Appl. Phys. **98**, 086103 (2005).
[42]B. G. Wang, J. Wang, and H. Guo, J. Appl. Phys. **86**, 5094 (1999).
[43]T. Christen and M. Büttiker, Phys. Rev. Lett. **77**, 143 (1996).